Line Protection Behaviour during Frequency Changes in Networks with high Inverter Based Resources Penetration

Roberto Cimadevilla*, Alberto Castañon, Javier García Villalobos

ZIV Automation, Parque Científico y Tecnológico de Bizkaia, 210. 48170 Zamudio, Bizkaia, Spain T: +34 94 452 20 03, www.ziv.es

*Contact Author: Parque Tecnológico, 210 48170 Zamudio (Vizcaya) - España Tel: +34 600570508 – Email: roberto.cimadevilla@zivautomation.com

ABSTRACT

Most Inverter-Based Resources (IBRs) are grid-following and rely on Phase-Locked Loop (PLL) units to track the system frequency. During fault conditions, PLL errors may occur, causing IBRs to inject currents at frequencies different from the nominal system frequency. This off-nominal frequency injection can affect the operation of several protection functions.

For distance protection, it produces rotations of the apparent fault resistance, impacting the line reactance response under resistive faults. Directional units may also be affected due to the phase shift between voltage and current caused by the frequency deviation. In line differential protection and external fault detectors based on directional comparison units, rotations occur between the local and remote currents, potentially compromising correct operation. This paper analyzes these effects across different polarizations of the line reactance, various types of directional units and differential and directional comparison units. The analysis is done through RTDS simulations using full-converter generator models. Solutions are proposed for units prone to misoperation under these conditions, improving the reliability of protection schemes in networks with high penetration of grid-following IBRs.

In addition, in networks with high penetration of grid-following IBRs, very high Rates of Change of Frequency (ROCOFs) may occur, affecting frequency tracking. Periods without adaptation of the sampling frequency to the system frequency can cause maloperations in certain units, such as voltage memory-based directional units or units based on prefault current. The impact of high ROCOFs on different protection functions, including distance, line differential protection and directional comparison is analyzed using oscillography from real events. Solutions are proposed for units that may operate incorrectly under these conditions.

Keywords: Distance, Line differential, ROCOF, PLL, fault resistance, directional, directional comparison

---

1.0 - INTRODUCTION

The growing integration of renewable energy sources has driven the extensive deployment of inverter-based resources (IBRs) in power systems. The majority of these IBRs operate using grid-following control schemes, aligning their output with the grid voltage through Phase Locked Loop (PLL) mechanisms. Although this strategy enables reliable performance under normal operating conditions, disturbances such as faults can introduce PLL errors, leading to deviations between the frequency of the injected currents and that of the network. These frequency mismatches directly affect several protection functions, including distance protection, directional elements, line differential protection and directional comparison units.

Distance protection is particularly impacted during resistive faults, as the frequency discrepancy between the grid and IBR currents produces a time-varying rotation of the apparent fault resistance. This can result in both underreach and overreach of the line reactance. Similarly, the frequency mismatch also influences line differential protection and directional comparison schemes, the latter

relying on the angular relationship between currents. Directional elements are also affected due to the frequency deviation introduced between voltage and current signals.

Furthermore, the high penetration of grid-following IBRs leads to reduced system inertia, thereby increasing the probability of rapid frequency excursions and elevated Rates of Change of Frequency (ROCOF). Such high ROCOF conditions pose challenges for conventional protection algorithms, especially those based on prefault quantities like memory voltage or prefault current. Under these circumstances, frequency tracking mechanisms may temporarily lose synchronism, resulting in measurement inaccuracies and incorrect phase relationships between voltage and current, which can ultimately trigger undesired protection operations.

This paper analyzes the performance of the aforementioned protection functions under off-nominal frequency conditions in systems with significant IBR penetration. The study focuses on the effects of PLL-induced frequency deviations and high ROCOF, using both simulation results for the first phenomena and real-case events to highlight the observed issues and suggest potential improvements in the behavior of the line reactance in distance protection, directional elements, line differential protection and directional comparison schemes.

2.0 - INFLUENCE OF IBR PLL ERRORS

IBR control systems typically rely on d–q components obtained through the Park transformation, which requires knowledge of the angle between the rotating d-axis and the stationary α-axis. In grid-following IBRs, control strategies generally align the d-axis with the grid voltage, enabling the decoupling of active (P) and reactive (Q) power components, where P is regulated by the $i_d$current component and Q by i_q. This alignment of the d-axis with the grid voltage is achieved by the PLL, following a commonly used simplified scheme such as the one illustrated in Figure 1 [2].

Any error in the PLL may lead to an incorrect estimation of the angle (θ) and frequency (ω), potentially causing the IBR to inject currents at a frequency that differs from that of the grid. This behavior can affect several protection functions, including line reactance under resistive faults, directional elements, differential protection and directional comparison units. To analyze this effect, a set of simulations is carried out. The simulated network is described in point 2.1.

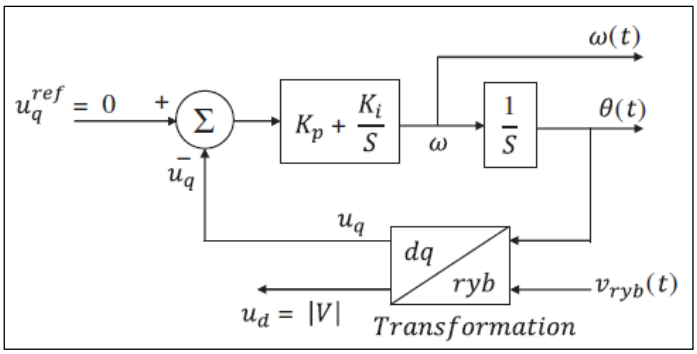


Figure 1. Simplified PLL diagram (reference [2])

It should be noted that frequency tracking does not resolve the issue, since frequency is typically measured from the voltage, whose frequency may differ from that of the current. The voltage frequency will depend on the magnitude of the voltage at the fault location, as the voltage at the IBR output is composed of the fault point voltage (at grid frequency) plus the voltage drop along the line (at the same frequency as the IBR current).

2.1 Simulation of PLL errors

The network modelled in RTDS is shown in Figure 2. The simulated data are shown in table 1

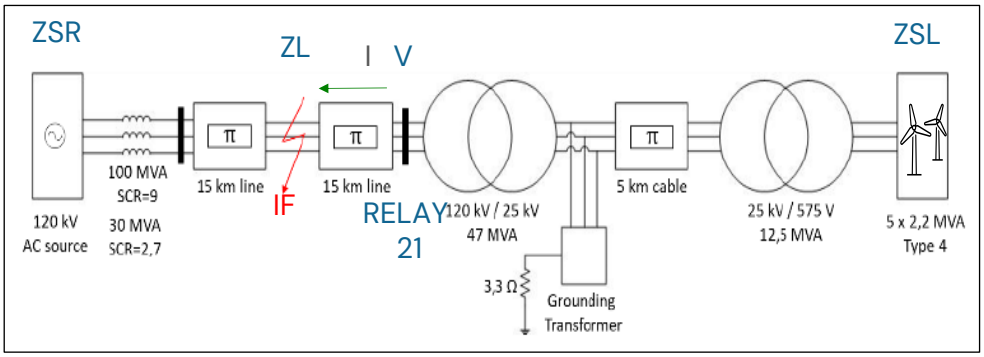


Figure 2 – Modelled network

Element	Parameter	Magnitude
AC Source	UAC	120 kV
	f	60 Hz
AC filter	R1	0,1 Ω
	L1	1 H
	R0	0,3 Ω
	L0	3 H
	S	100 MVA
15 km line	R1	0,176 Ω/km
	L1	1,57e-3 H/km
	C1	0,0127e-6 F/km
	R0	0,42 Ω/km
	L0	3,82e-3 H/km
	C0	0,007e-6 F/km
HV-MV transformer	V1	120 kV
	V2	25 kV
	S	47 MVA
5 km cable	R1	0,1153 Ω/km
	L1	1,05e-3 H/km
	C1	11,33e-9 F/km
	R0	0,413 Ω/km
	L0	3,32e-3 H/km
	C0	5,01e-9 F/km

MV-LV transformer	V1	25 kV
	V2	575 V
	S	12,5 MVA
Type 4 wind farm	P	5*2 MW

Table 1 – Modelling data

Permanent PLL errors are forced during the fault duration. Internal faults at 50% of the protected line are considered.

2.2 Influence on line reactance with resistive faults

Before checking the influence of the PLL errors on distance protection, a review of the influence of the fault resistance on the line reactance is done.

2.2.1 Review of the influence of fault resistance on the line reactance

The voltage measured by a distance relay located at point A, protecting line AB, for the internal fault shown Figure 3 can be expressed as: V=IL*Z1LF+IF*RF, where IL is the local current, Z1LF is the positive-sequence line impedance up to the fault point, IF is the current that flows through the fault resistance (sum of IL and IR) and RF is the fault resistance.

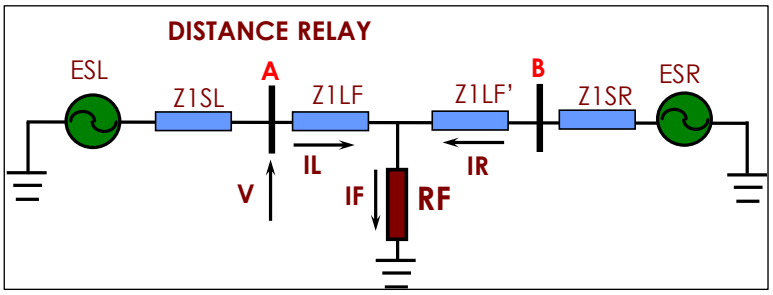


Figure 3 – Circuit for internal resistive fault

Due to the load flow and non-homogeneity of the system, IL and IR are phase-shifted, which implies that IL and IF are also phase-shifted. The angle between IL and IF is called α. It can be positive or negative.

Figure 4 plots the voltage and line reactance in a voltage diagram (R*I-X*I diagram). Zr represents the zone reach. It can be observed that, due to the fault resistance, the fault point F is moved to Fr. If the line reactance stays horizontal and α is negative there can be an overreaching effect. Conversely, if α is positive an underreaching effect may appear.

Suitable polarization phasors are required for the line reactance, in order to introduce a tilt that accounts for the voltage drop across the fault resistance (see Figure 5), thereby avoiding the previously mentioned effects. Reference [1] presents appropriate polarization phasors that incorporate a compensating factor, denoted as Kn, which depends on the local source impedance and ensures correct operation in the presence of IBRs: FPOL=In*Kn, n=0, 1, 2 (symmetrical components); Kn=f(ZnSL); ZSL (local source impedance).

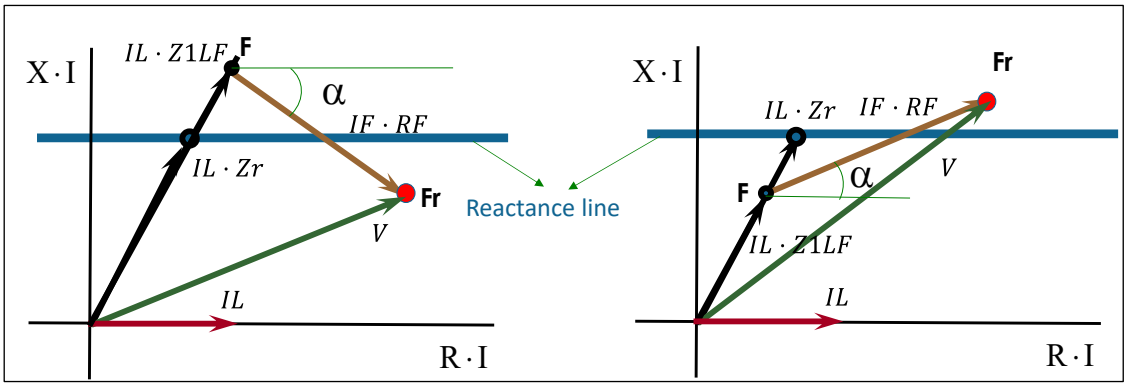


Figure 4 – Effect of fault resistance on static line reactance (voltage diagram)

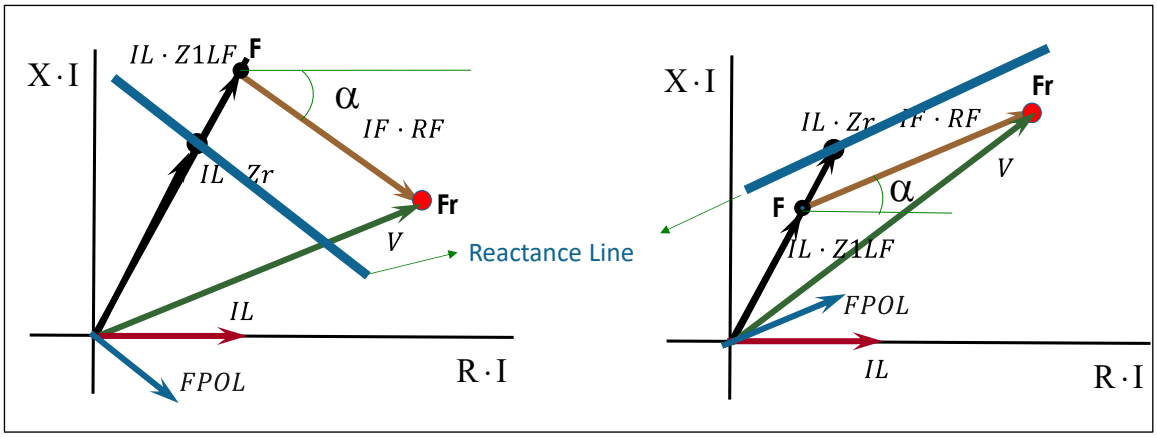


Figure 5 – Effect of fault resistance on dynamic line reactance (voltage diagram)

2.2.2 Influence on the line reactance: simulation results

If, in Figure *3,* ESL is an IBR and a PLL error is present, the frequencies of IL and IR will differ. As a result, the frequencies of IL and IF will also be different, causing the angle α to vary over time. Do the polarization phasors defined in reference [1] follow α?. Table 2 presents the simulation results. The advanced phasors described in reference [1] that use the compensating factor are highlighted in blue, whereas the conventional polarization phasors, such as I2, Iph-Iph_pf (pf meaning prefault) are shown in black. It can be checked that the advanced phasors perform correctly, while the conventional ones fail.

FPOL	FAULT TYPE		
	AG	AB	ABG
I2	FAIL	FAIL	N/A
I2*K2	OK	OK	N/A
Iph-Iph_pf	FAIL	N/A	N/A
Iphph-Iphph_pf	N/A	FAIL	FAIL
(I1-I1pf)*K1-I2*K2	N/A	N/A	OK
(I1-I1pf)*K1	OK	OK	OK

Table 2 – Results with advanced and conventional polarization phasors

The angle between the polarization phasor and the current flowing through the fault resistance (IF) is shown in Figure 6 and Figure 7 for AG and ABG faults, respectively. The angle corresponding to the advanced polarization phasor is shown in red, while those associated with the conventional phasors (Iph or Iphph and Iph-Iph_pf or Iphph-Iphph_pf) are represented in blue and green. It can be observed

that the angle for the advanced polarization phasor remains close to zero and does not vary over time. In contrast, the angle for the conventional polarization phasors is significantly different from 0° and varies with time. This behavior may lead to underreach or overreach effects in the line reactance.

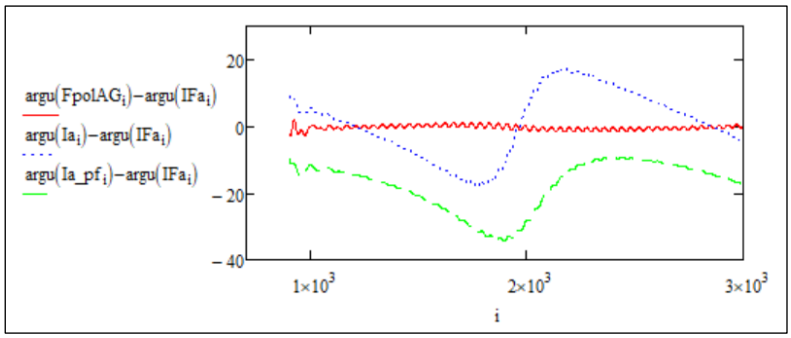


Figure 6 – Angle between line reactance polarization phasor and current flowing in the fault resistance for AG fault

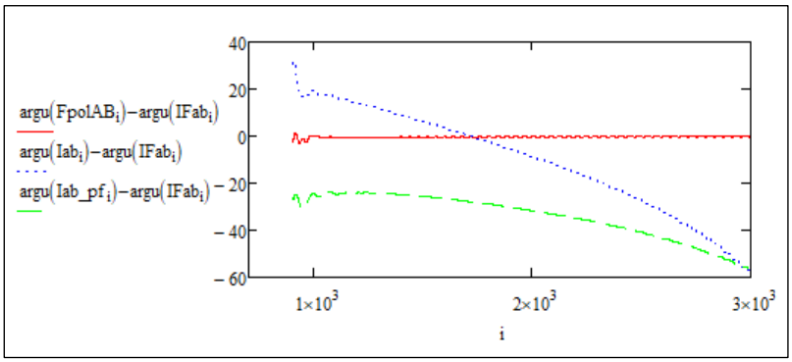


Figure 7 – Angle between line reactance polarization phasor and current flowing in the fault resistance for ABG fault

2.3 Influence on directional units

The frequency difference between the IBR currents and the grid voltage introduces a variation in the angle between these quantities, which may affect the operation of directional units. Figure 8 and Figure 9 illustrate the angle difference between the polarization (voltage) and operating (current) phasors for different directional elements: negative-sequence, positive-sequence, and zero-sequence, in the case of an ABG fault. Different control strategies for negative-sequence current (I2) injection are considered: the first follows the Spanish Grid Code, which requires the injection of a purely reactive I2 current [3], while the second injects I2 to remove active power oscillations [4].

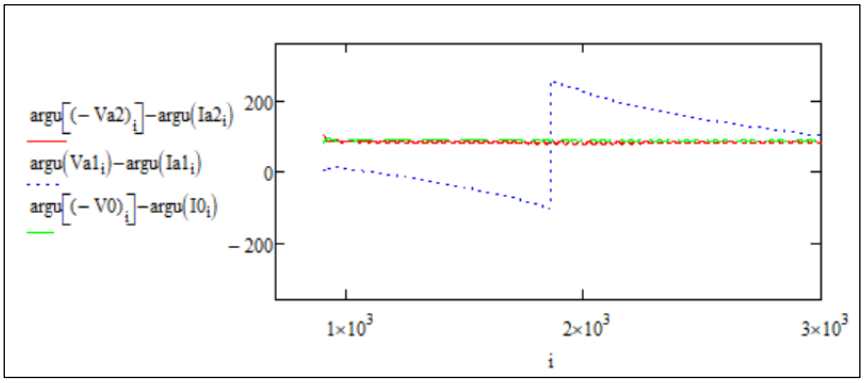


Figure 8 – Angle between polarization and operation phasors for 67Q, 67P and 67N units for ABG fault (control based on Spanish Grid Code)

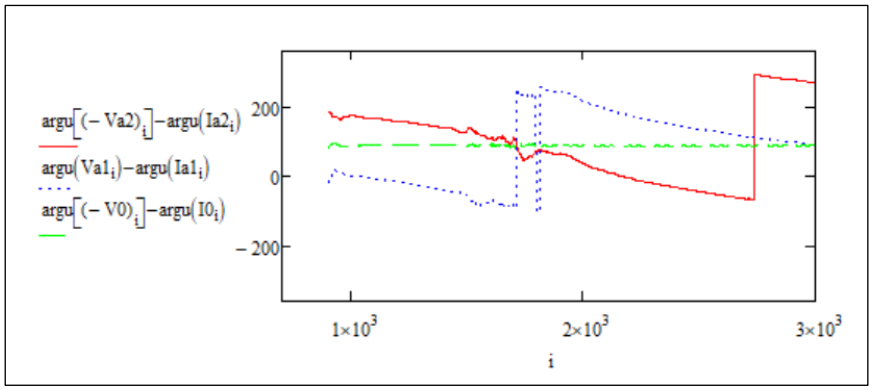


Figure 9 – Angle between polarization and operation phasors for 67Q, 67P and 67N units for ABG fault (control to remove P oscillations)

It can be observed that the 67N unit operates correctly. This is because both I0 and V0 are determined by the grid. The IBR does not contribute to I0; instead, this current is supplied by the grid through the DYn transformer. As a result, the voltage drop from the IBR to the fault location also remains at the grid frequency.

It can also be seen that, when applying the control strategy defined by the Spanish Grid Code, the 67Q unit operates properly, since the control aims to maintain I2 at 90° with respect to V2, as illustrated in Figure 8. However, for other control approaches, such as those intended to keep active power constant, I2 depends not only on V2 but also on V1 [4]. Consequently, the angle between V2 and I2 varies over time, as shown in Figure 9.

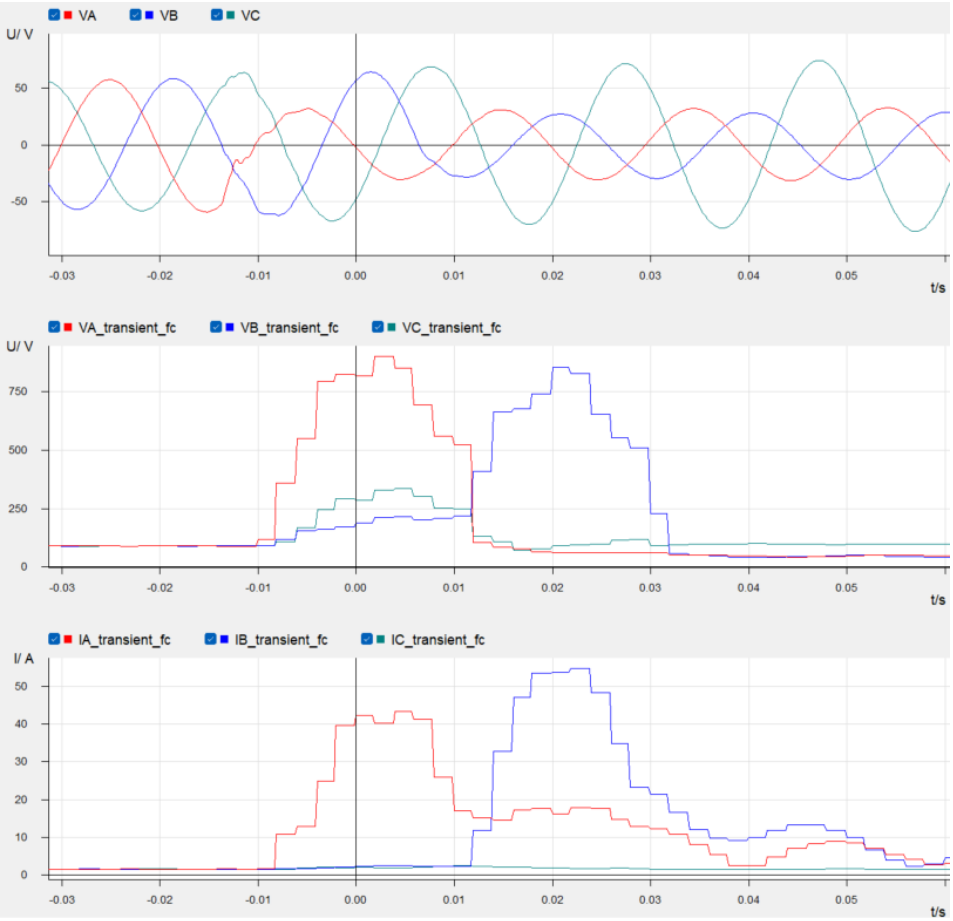


Figure 10 – Transient monitor activation during evolving fault.

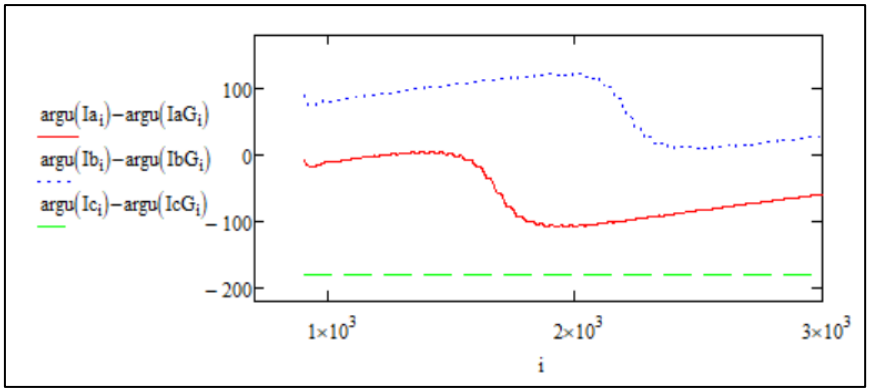
If the fault involves ground, the use of the 67N unit is clearly required. However, for faults not involving ground, it can be observed that the 67Q and 67P units may maloperate. In breaker-and-a-half arrangements, a directional element based on the two CT currents (see reference [5]) can be applied. In contrast, for single-breaker configurations, if a frequency difference between current and voltage is detected, the output of the directional unit, evaluated two cycles after fault inception, can be latched, as the direction indication at that moment is reliable due to the small phase shift between voltage and current caused by the slip.

Nevertheless, if the fault evolves, the direction indication must be recalculated. This condition can be identified using a transient monitor, such as the one described in reference [6]. As long as no new fault occurs, the transient monitor remains inactive. Figure 10 illustrates the activation of the transient monitor during an evolving fault from AG to ABG. It can be observed that, at the start of the fault, the transient monitor values for VA and IA increase. When the fault evolves to ABG, the transient monitor values for VB and IB also rise. Once the steady-state conditions are reached, the transient monitor values associated with the faulted phases become very low

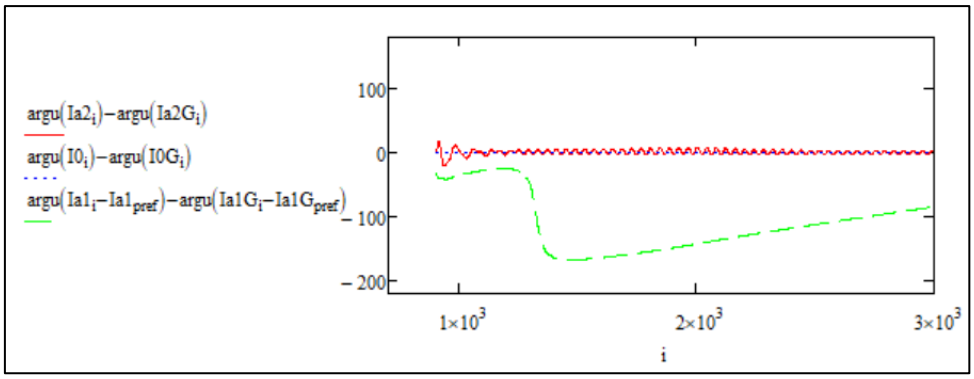
2.4 Influence on differential unit and directional comparison units

The frequency difference between IBR and network currents makes the angle between both currents change with time. Figure 11.a and Figure 11.b show the angle between the phase currents and between the pure fault sequence currents, respectively, for a control following the Spanish Grid Code. It can be seen that the angle between the phase currents and between the pure fault positive-sequence currents varies with time. This can make the directional comparison units (or phase comparison units) that use this angle detect an external fault. However, the angle between the zero-sequence currents keeps close to 0º, because the zero-sequence current at IBR side is provided by the grid and, therefore, it has the same frequency as the zero-sequence current on the grid side. This allows the zero-sequence directional comparison unit to work properly.

The angle between the negative-sequence currents also remains close to 0º. This is due to the IBR control, as it tries to maintain the angle between -V2 and I2 at 90º, resulting in a near 90° angle of the negative-sequence source impedance on the IBR side. Since the angle of the negative-sequence source impedance at the grid side is also close to 90º (assuming synchronous generation), as is the angle of the negative-sequence line impedance, the angle between the -V2f (negative-sequence voltage at the fault point) and I2 on both IBR and grid side is also close to 90º. This results in an angular relationship between I2 at IBR side and I2 at the grid side that is close to 0º.



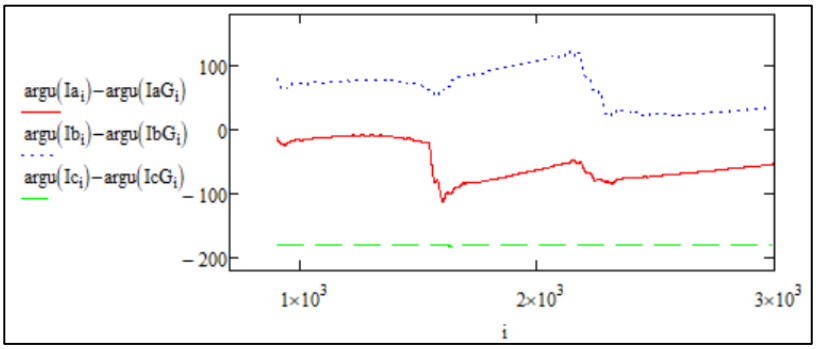
a. Phase currents



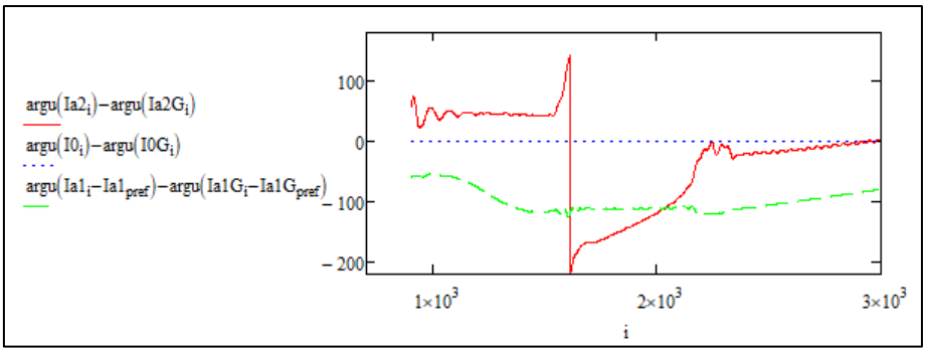
b. Pure fault sequence currents

Figure 11. Angle between currents at IBR and grid side for IBR control based on the Spanish Grid Code

Due to the explained angle change between the phase currents and the positive-sequence pure fault currents at both ends of the line, the corresponding differential currents will change over time, although they will not reach zero, due to the magnitude difference between the local and remote currents. Therefore, once the differential unit has tripped, it will not reset. The external fault detector described in reference [9] is based on three units: a differential unit with instantaneous values, a phase directional comparison unit, and a pure fault positive-sequence directional comparison unit. The latter two units, since they rely on the angle difference between the currents at both ends of the line (phase currents and positive-sequence pure fault currents, respectively), can temporarily activate the external fault signal. This will not block the differential unit, as the recommended blocking logic follows a "3 out of 3" condition, and the first unit, differential unit with instantaneous values, will not activate the external fault, due to the magnitude difference between local and remote currents. In any case, if setting a "2 out of 3" logic is desired, the pure fault positive-sequence directional comparison unit could be replaced with a zero-sequence directional comparison unit if a ground fault is detected. Alternatively, the same latching strategy for the directional units, based on the transient monitor, can also be applied to the positive-sequence directional comparison unit if the fault does not involve ground. The condition for latching this unit can be the same as that used for the directional units: a frequency difference between the voltage and current. Note that this condition will not be met on the grid side. However, if trip permanence is guaranteed on the IBR side and a direct transfer trip is enabled, the trip on the grid side will also remain active for the entire duration of the fault.



a. Phase currents



b. Pure fault sequence currents

Figure 12. Angle between currents at IBR and grid side for IBR control designed to remove P oscillations

Figure 12.a and Figure 12.b show the angle between the phase currents and between the pure fault sequence currents, respectively, for a control designed to remove P oscillations. Note that the angle between positive-sequence pure fault currents and between negative-sequence currents at both ends of the line varies with time. The control does not try to make the angle between -V2 and I2 at the IBR side close to 90º and the injection of I2 depends not only on V2 but also on V1 [4]. Also observe that the angle between the zero-sequence currents keeps close to 0º. The same solutions mentioned before, for the control following the Spanish Grid Code, can be applied in this case: replacing positive-sequence directional comparison unit by zero-sequence directional comparison unit for ground faults and latching the positive-sequence directional comparison unit, using the frequency difference between voltage and current and the transient monitor, for faults not involving ground.

3.0 - INFLUENCE OF HIGH ROCOF IN NETWORKS WITH HIGH IBR PENETRATION

While the previous section focused on frequency deviations caused by local PLL errors, this section analyzes the influence of high IBR presence on fast frequency changes.

In networks with high IBR penetration, system inertia may be reduced, as most IBRs operate in grid-following mode and therefore do not contribute to inertia. This can lead to high ROCOF values during frequency variations. It should be noted that, during unstable power swings, ROCOF may be even higher due to transient conditions.

Protection relays typically incorporate frequency tracking algorithms that adjust the sampling frequency to match the network frequency. This frequency tracking helps to reduce measurement errors and mitigate angle deviations.

3.1 Measurement errors

When the DFT sampling window does not correspond exactly to one network cycle, the waveform is no longer periodic within the window. This introduces discontinuities, leading to errors in the DFT output. The DFT computes the real and imaginary components by multiplying the measured waveform by cosine and sine waveforms, respectively, and summing the resulting products [8]. When the sampling frequency is not synchronized with the network frequency, a mismatch arises between the frequency of the measured waveform and that of the cosine and sine signals.

As an example, consider a measured waveform $x(t)$at 52 Hz (with magnitude equal to 1 and angle set to 0°), while the sampling frequency is tracked at 50 Hz:

$x(t) = cos(2\pi 52t)$; cos(t)=$cos(2\pi 50t)$; sin(t)=$sin(2\pi 50t)$

If we consider the sum of the product x(t)*cos(t) as the integral of this product, the real part will be:

$$Re(t) = \frac{2}{T} \cdot \int_{t-T}^{T} cos(2\pi 52t) \cdot cos(2\pi 50t) \cdot dt$$

Where T is the period for 50 Hz. As, cos(a)*cos(b)=1/2*[cos(a-b)+cos(a+b)]

$$Re(t) = \frac{2}{T} \cdot \int_{t-T}^{T} 0.5 \cdot cos(2\pi 2t) \cdot dt + \frac{2}{T} \cdot \int_{t-T}^{T} 0.5 \cdot cos(2\pi 102t) \cdot dt$$

Figure 13 (left) shows the real part in red, the first term of the sum (Re1(t): integral of the cosine at 2 Hz) in blue, and the second term of the sum (Re2(t): integral of the cosine at 102 Hz) in green. Since 2 Hz does not correspond to a DC component, its integral over T exhibits a slow oscillation (it can be shown that the resulting frequency is 2 Hz). Because 102 Hz is not an exact multiple of 50 Hz, its integral over T does not equal zero, as the positive and negative areas do not fully cancel each other out. As a result, its output depends on the waveform sampling instant, producing a small ripple around zero. If the measured waveform is at 50 Hz, the real part and the two summation terms are shown in Figure 14 (left). A similar reasoning can be applied to the imaginary part, noting that cos(a)*sin(b)=1/2*[sin(b+a)-sin(b-a)] (see Figure 13 and Figure 14 right).

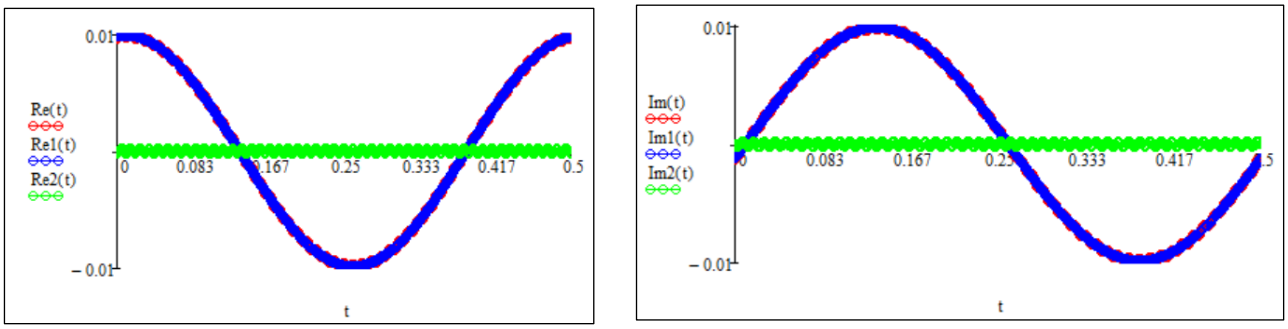


Figure 13 – Real (left) and Imaginary (right) parts of waveform with 52 Hz sampled with sampling frequency tracked to 50 Hz

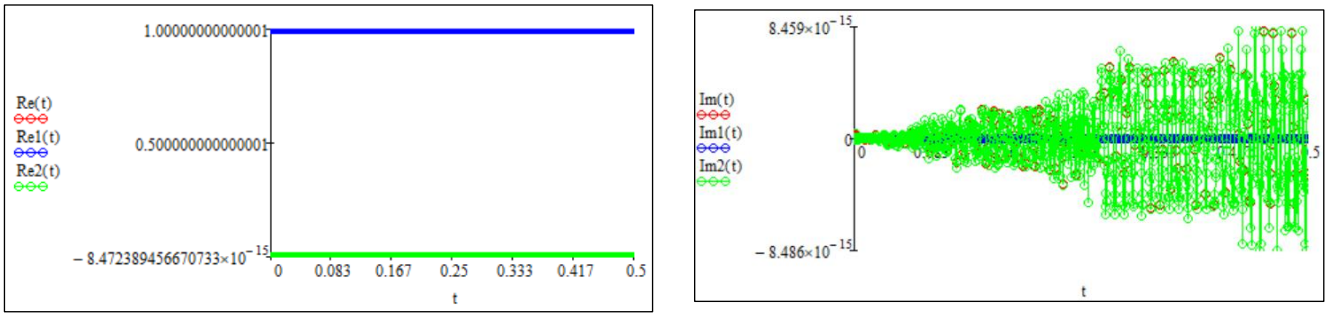


Figure 14 – Real (left) and Imaginary (right) parts of waveform with 50 Hz sampled with sampling frequency tracked to 50 Hz

The magnitude of the phasor is given by $\sqrt{(Re)^2 + (Im)^2}$. The magnitude of the 102 Hz component will exhibit an oscillation and remain close to zero. The magnitude of the 2 Hz component does not oscillate, but shows an attenuation of approximately 0.997, corresponding to an error of about 0.3%. This value results from the integration of the 2 Hz component over the interval T.

For example, for t=20 ms, $Re1(0.02) = \frac{2}{T} \cdot \int_{t-T}^{T} 0.5 \cdot cos(2\pi 2t) \cdot dt = \frac{1}{T} \cdot [\frac{\sin(2\pi \cdot 2 \cdot T) - \sin(2\pi \cdot 2 \cdot (t-T))}{2\pi \cdot 2}] = \frac{\sin(2\pi 2 \cdot 0.02) - \sin(0)}{4\pi \cdot 0.02} = \frac{\sin(0.08\pi)}{0.08\pi} \approx 0.990$; similarly, Im1(0.02)≈0.125. Therefore $\sqrt{(Re)^2 + (Im)^2} \approx 0.997$.

3.2 Angle change

The angle provided by the DFT will vary over time because the cosine and sine waveforms used by the DFT and the measured waveform have different frequencies. This affects protection units that rely

on prefault quantities, since the angle of these quantities changes with respect to the angle of the current quantities:

- Prefault voltage, such as in memory voltage directional units or memory voltage Mho characteristics. Typically, memory voltage is only used once a fault is detected (fault detector activation), and the positive-sequence voltage is low if the line is not series compensated.
- Prefault current, such as phase selectors based on positive and negative sequence currents, line reactance polarization based on pure fault current, or directional comparison and differential units based on pure fault current, such as those using positive-sequence pure fault current [9], etc.

3.3 Frequency tracking delays

Frequency tracking cannot be activated instantaneously, as it must distinguish frequency variations from other events such as phase shifts. To achieve this, several consecutive frequency measurements are typically required to differentiate between these conditions [7]. If the frequency variation is very fast, frequency tracking usually delays the adjustment of the sampling frequency, since it is designed for a maximum ROCOF (around 15 Hz/s in the relay under study). When the ROCOF exceeds this limit, a longer time is needed to confirm that the event corresponds to an actual frequency change.

It should be noted that, during the period in which the sampling frequency is not properly tracked, measurement errors and phase slips between voltage and current may occur.

3.4 Real events

3.4.1 Event 1

Figure 15 shows a real event in which, due to a high IBR penetration in the network, high ROCOF occurred during an unstable power swing. The ROCOF measured by the relay, which, by default uses 7 half-cycles derivation time, is higher than 70 Hz/s. FREQ is the frequency measured by the relay and FREQ_PLL is the tracked frequency. As the ROCOF is higher than the maximum value, FREQ_PLL is not tracked to FREQ during around 70 ms. During this period, on the one hand, a high voltage and current phase shift is generated and, on the other hand, errors in the current measurement occur. These errors activate the fault detector, which, during power swings, is based on I0 and I2 levels and ΔI0 and ΔI2 values.

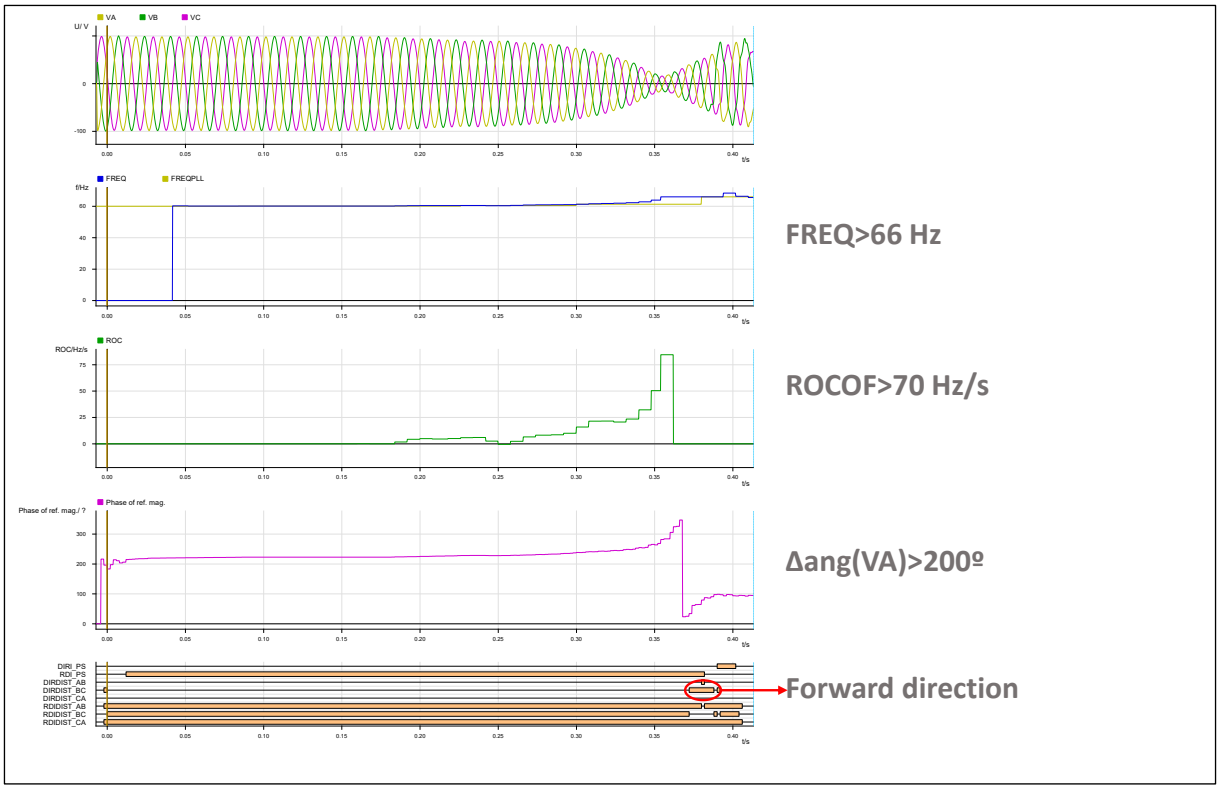


Figure 15 – Unstable power swing with high ROCOF (event 1)

3.4.1.1 Impact on memory voltage directional unit

As the voltage drops to low values, memory voltage is used in the distance directional unit. Due to the high phase slip during this period (Δang(VA)>200º) the use of memory voltage causes the directional unit to issue an incorrect output. It should be noted that the impedance seen by the relay during the unstable power swing moves through the third and fourth quadrants; however, since the directional unit transiently indicates a forward fault, zone 1 is tripped. The moment at which the impedance enters zone 1 can be observed in Figure 16.

It should also be noted that even if memory voltage phase-shift compensation, as described in reference [7], is applied, the incorrect operation of the memory-voltage-based directional unit cannot be fully prevented.

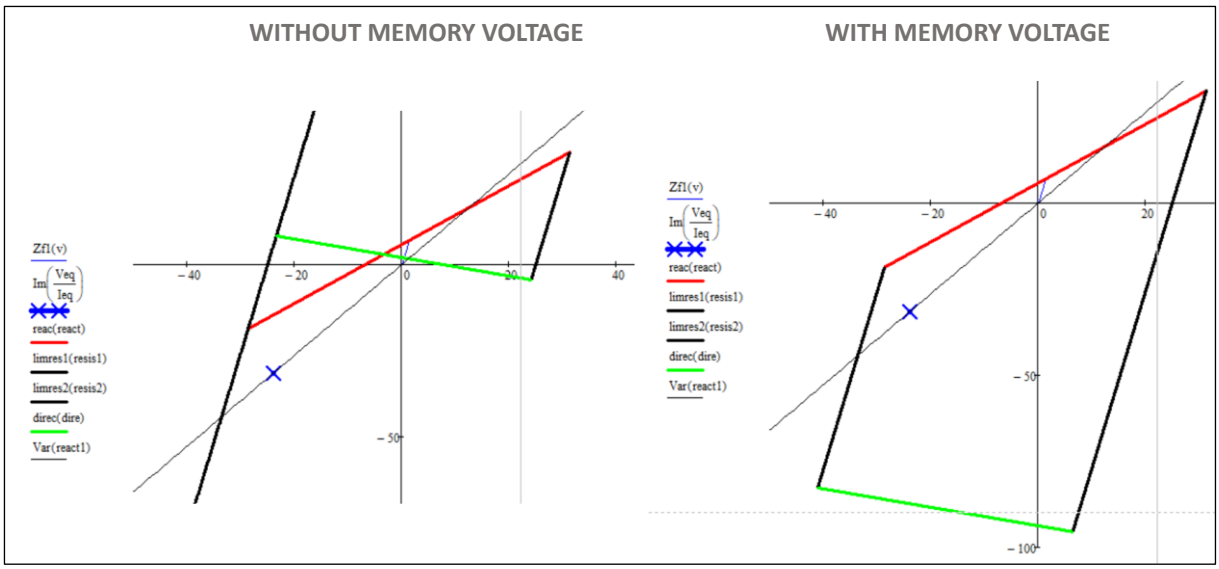


Figure 16 – Zone 1 quadrilateral characteristic and impedance seen with and without using memory voltage during the unstable power swing (event 1)

3.4.1.2 Impact on line differential and directional comparison units

Figure 17 shows the angle difference between the positive-sequence pure fault currents at both ends of the line, as measured by a line differential relay during the power swing in Event 1. Due to the period in which the sampling frequency is not tracked to the network frequency, as previously explained, the fault detector, based on I2 and I0 levels and on ΔI2 and ΔI0 values, is activated. This triggers the selection of a prefault current to construct the positive-sequence pure fault current, whose angle varies over time due to the frequency difference between the “prefault” and “fault” currents. However, this does not cause the positive-sequence pure fault directional comparison unit to declare an internal fault, since the angles of both local and remote currents change at the same rate, resulting in an angle difference close to 180°.

On the other hand, the differential current, calculated with instantaneous values, as described in reference [9], keeps close to zero (see Figure 18).

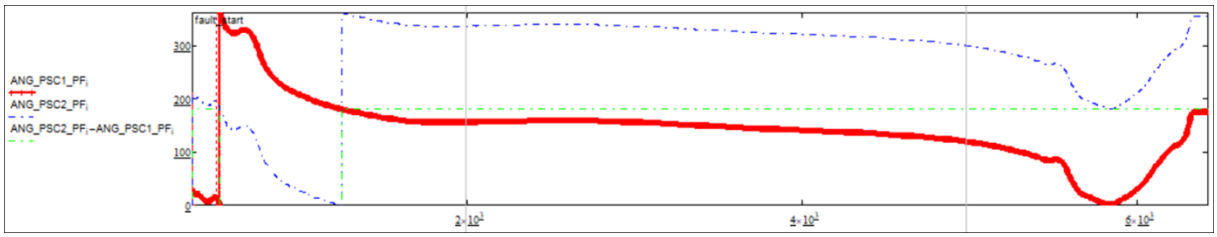


Figure 17 – Angle of positive-sequence pure fault current at both ends of the line measured by a line differential relay and its difference (event 1)

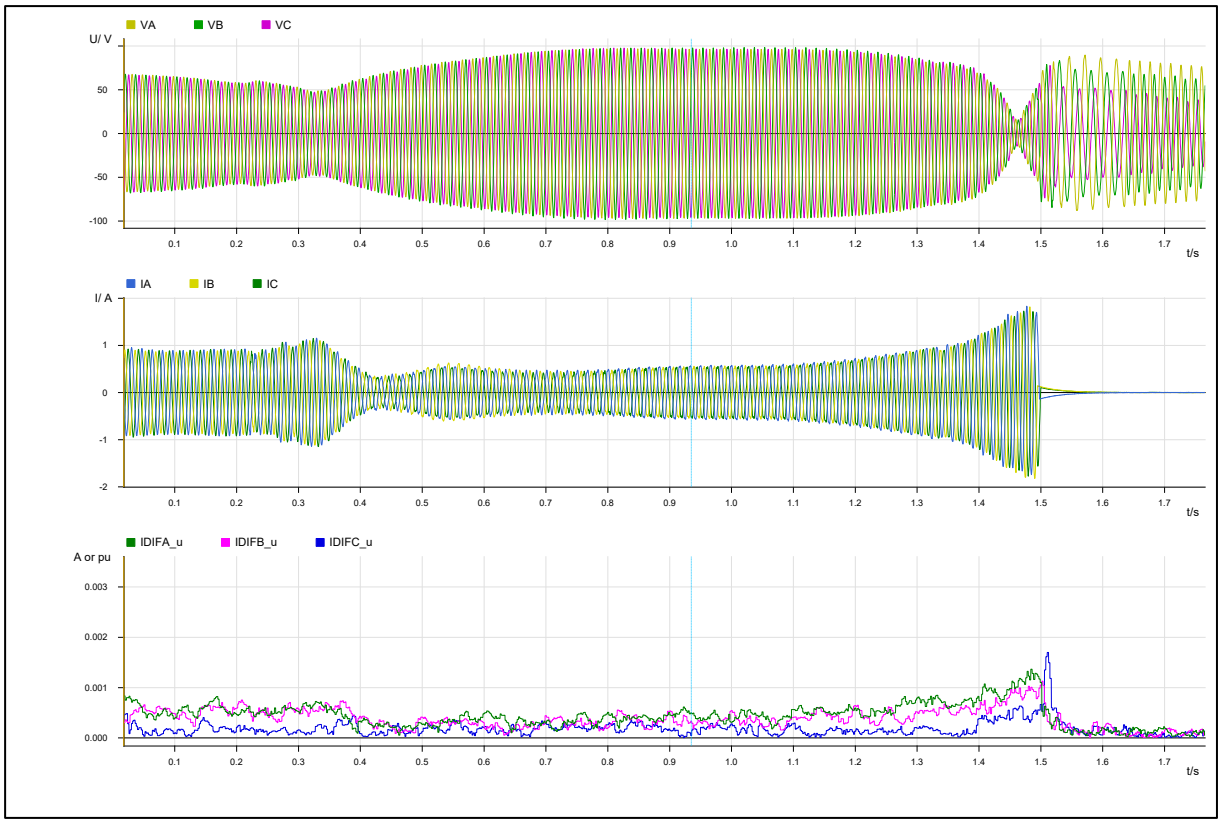


Figure 18 – Phase voltages, currents and differential currents measured by the line differential relay (event 1)

3.4.2 Event 2

Figure 19 shows another real event in which a high ROCOF was also generated during an unstable power swing.

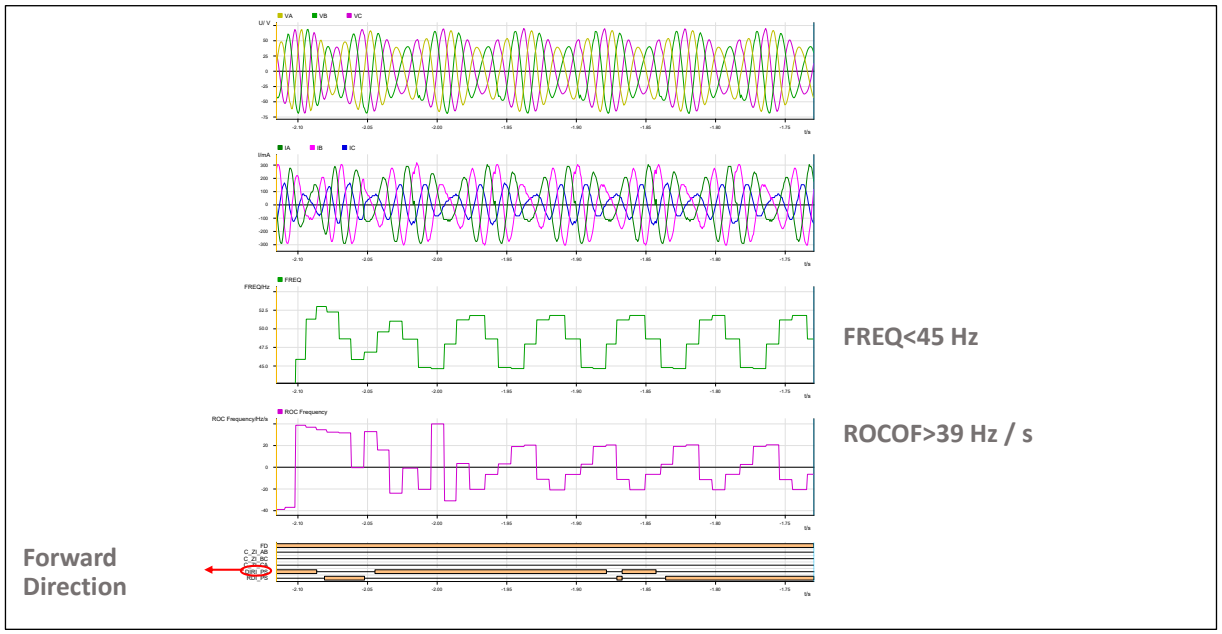


Figure 19 – Unstable power swing with high ROCOF (event 2)

3.4.2.1 Impact on memory voltage directional unit

Zone 1 tripped due to an incorrect directional unit operation caused by the use of memory voltage. The behavior is similar to that observed in the first event. Figure 20 shows zone 1 quadrilateral characteristic with and without using memory voltage.

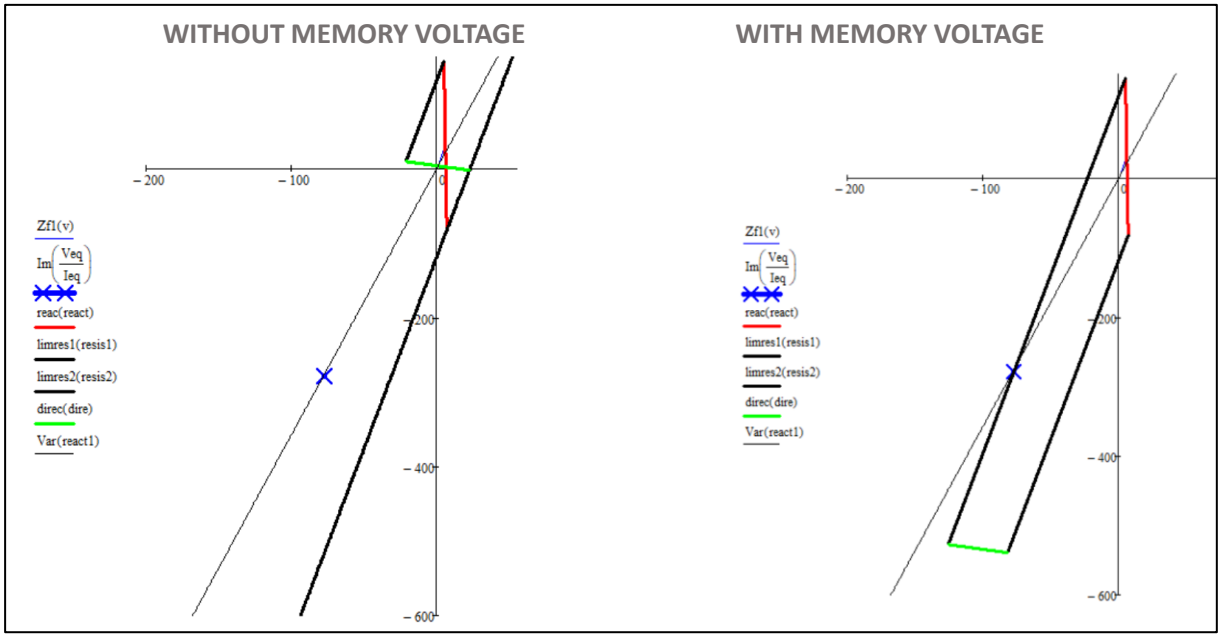


Figure 20 – Zone 1 quadrilateral characteristic and impedance seen with and without using memory voltage during the unstable power swing (event 2)

3.4.2.2 Impact of line differential and directional comparison

Figure 21 shows the angle difference between the positive-sequence pure fault currents at both ends of the line, as measured by a line differential relay during the power swing in Event 2. It can be observed that this angle remains close to 180°. The same conclusions drawn for the behavior of the positive-sequence pure fault directional units and line differential protection during Event 1 also apply to Event 2.

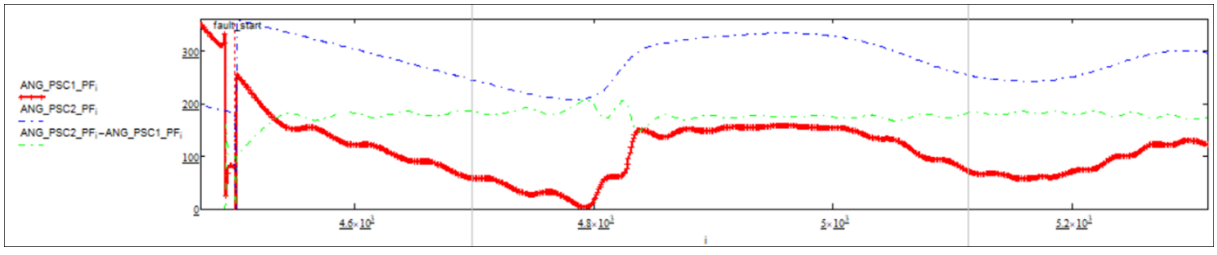


Figure 21 – Angle of positive-sequence pure fault current at both ends of the line measured by a line differential relay and its difference (event 1)

4.0 - CONCLUSION

The increasing penetration of IBRs introduces significant challenges for conventional protection functions, particularly under off-nominal frequency conditions. This work has demonstrated that PLL errors can lead to discrepancies between the frequencies of IBR and grid currents, as well as between voltage and current frequencies at the IBR side.

This results in a time-varying rotation of the apparent fault resistance, affecting the behavior of the line reactance. Simulation results confirm that advanced polarization techniques based on compensating factors linked to source impedance provide a robust solution for line reactance. These methods effectively track the dynamic behavior of the fault resistance angle.

Directional elements are also impacted by frequency discrepancies between voltage and current. While zero-sequence directional units remain reliable due to their dependence on grid-supplied quantities, positive and negative-sequence units may experience instability depending on the IBR control strategy. Practical mitigation measures include the use of alternative directional principles (e.g., current-only methods in specific configurations), controlled latching of directional decisions, and transient monitoring to detect fault evolution.

Line differential and directional comparison units are also affected due to the angle variation between local and remote currents. Line differential protection maintains correct operation due to the magnitude difference between local and remote currents. The zero-sequence directional comparison unit maintains the internal fault indication because the angle difference between zero-sequence currents remains, for the internal faults, close to 0°, as both local and remote currents are supplied by the grid. For positive-sequence directional comparison, a controlled latching approach based on the frequency difference between voltage and current, together with a transient monitor, is proposed.

The reduction of system inertia associated with high IBR penetration leads to elevated ROCOF values during disturbances, disrupting frequency tracking algorithms and introducing phasor estimation errors and significant phase shifts. These effects can trigger incorrect operation of distance protection, particularly when memory voltage is used. Disabling or supervising memory voltage usage under high ROCOF conditions, combined with adaptive latching strategies, has proven effective in preventing false trips.

It is shown that the impact of high ROCOF during power swings does not affect line differential protection based on instantaneous values, as the differential current remains very low. It also does not affect pure fault directional comparison units, since the rate of change of the angle is the same at both ends of the line. The angle difference between currents at both ends of the line keeps close to 180º.

Overall, the study highlights that conventional protection algorithms must be adapted to account for the dynamic and frequency-sensitive behavior introduced by IBRs. Enhanced polarization techniques, improved directional logic, and ROCOF-aware supervision are key measures to ensure dependable and secure protection performance in low-inertia power systems.

7 REFERENCES

[1] A. Castañon, R. Cimadevilla, P. Eguia, E. Torres and R. Ibarra, "Impact of Wind Generation on Line Protection," PAC World Conference 2021, On Line, 2021.

[2] Nasser Tleis, Power System Modelling and Fault Analysis, theory and practice, second edition

[3] R.E.E., P.O. 12.2: Instalaciones de generación y demanda: requisitos mínimos de diseño, equipamiento, funcionamiento, puesta en servicio y seguridad, 2018

[4] R. Cimadevilla, A. Castañón, P. Eguia, E. Torres, “Abnormal Fault Patterns in the Presence of Inverter Based Generation and Their Effect on Line Protection”, DPSP Europe, 2025

[5] R. Cimadevilla, “Protection for Breaker and a Half or Ring Bays”, SEAPAC, Melbourne, March 2009

[6] A. G. Phadke, T. Hlibka, M. Ibrahim, M. G. Adamiak, 'A microcomputer based Symmetrical Component Distance Relay', Proceedings of PICA, April, 1979

[7] R. Cimadevilla, R. Quintanilla, S. Ward “Adapting Protection to Frequency Changes”, WPRC, October 2005

[8] R. Cimadevilla, “Fundamentos de la medición de sincrofasores”, ERIAC 2009

[9] Instructions Manual Line Differential Protection model DLF: M0DLFA1907Iv44 (03/2026)

5.0 - BIOGRAPHICAL DATA

Roberto Cimadevilla graduated in Electrical Engineering from the Superior Engineering College of Gijón, Spain, in 2001. He completed his final-year project at the University of Dundee, Scotland, and obtained a Master’s degree in “Analysis, Simulation and Management of Electrical Power Systems” from the University of the Basque Country, Spain. He joined ZIV in 2003, where he has actively contributed to the development of several protection and control devices, including distance, transformer differential, line differential, and feeder relays. He has held various technical and management positions within the company and is currently Manager of the Application Engineering Department. He has authored more than 35 papers, teaches in the Master’s Program in Industrial Engineering at the University of Deusto, is an IEEE member, and has participated in several CIGRE working groups.

Alberto Castañón was born in Tixtla, México en 1990. Graduated and Electromechanical Engineer by the Monterrey Institute of Superior Technological Studies in 2014. Between 2014 and 2019 worked as an Electrical Engineer for General Electric in the Gas Turbine Power business. In 2009 he studies a Masters about Renewable Energy Integration on the Electrical Grid by the Basque Country University, Spain, writing its final thesis by ZIV, which he joined as an application engineer up to now, working mainly on distance and differential protections and renewable energy impact on protection engineering.

Javier Garcia-Villalobos received the Automatic and Industrial Electronics Engineering degree and the Integration of Renewable Energies in the Electrical System master’s degree from the University of the Basque Country, Spain, in 2010 and 2011, respectively. He obtained the PhD degree from the University of the Basque Country in 2016 with his thesis: “Optimized charging control method for plug-in electric vehicles in LV distribution networks”. Javier joined ZIV in 2017 as Application Engineer. He is the author or coauthor of 3 scientific papers in indexed journals (his h-index is 6) and more than 10 publications for scientific journals and book chapters. Additionally, he has presented/participated in more than 20 international conferences. Currently, he is member of the working groups IEC TC95/MT4 and CIGRE WG B5.71.